Electrochimica Acta 55 (2010) 1709–1719

Contents lists available at ScienceDirect

Electrochimica Acta

journal homepage: www.elsevier.com/locate/electacta

Electrocatalysis of oxygen reduction on carbon-supported PtCo catalysts prepared by water-in-oil micro-emulsion

Qinggang He, Sanjeev Mukerjee*

Department of Chemistry and Chemical Biology, Northeastern University, 360 Huntington Avenue, Boston, MA 02115, USA

ARTICLE INFO

Article history:
Received 23 August 2009
Received in revised form 23 October 2009
Accepted 25 October 2009
Available online 1 November 2009

Keywords:
Platinum
Cobalt
Micro-emulsion
Reverse micelles
ORR
Peroxide yield
Surface composition effect

ABSTRACT

Synthesis of carbon-supported PtCo/C using micro-emulsion method including simultaneous procedure and sequential procedures in both acid and alkaline media was reported. UV–vis and electron microscopy were used to characterize the formation, surface morphology and distribution of PtCo nanoparticles. Crystallite structure of catalysts was analyzed from XRD patterns. Catalytic properties of PtCo/C catalysts synthesized were compared with commercial Pt/C using RDE based on both mass activity (MA) and specific activity (SA). PtCo/C catalysts prepared in both acidic and basic conditions showed better performance than commercial Pt/C catalyst. High-temperature heat treatment was found useful only to PtCo/C by sequential procedure. The peroxide yield was also explored using RRDE technique. The H_2O_2 yield results were correlated with SA and *R* values (ratio of charge transferred about Co and Pt on the surface of catalyst) obtained from CVs in 1 M KOH solution. A sacrificial Co oxidized effect on impediment of adsorption of OH may cause higher catalytic properties and higher H_2O_2 yield to Pt base alloy catalysts.

1. Introduction

Proton exchange membrane fuel cells (PEMFCs) have been developing for transport applications as well as for stationary and portable applications due to their high energy density, high efficiency, relatively low operating temperature and low emission of pollutants [1]. Low performance of the oxygen reduction reaction at the cathode and membrane degradation are two remarkable obstacles to the highly successful application in transportation markets of PEM fuel cells [2–6]. Various Pt based alloy catalysts [7–13] have been developed and show enhanced catalytic activity compared to Pt/C towards oxygen reduction reaction in PEMFC. The first reported systematic study of the ORR on Pt alloys was conducted by Mukerjee et al. [14,15]. Five binary alloys of Pt with first row transition elements ranging from Cr to Ni were investigated. All the alloy electrocatalysts were found to enhance ORR activity albeit to different extents. Comparison of ORR activity as *iR* corrected Tafel plots for oxygen reduction taken at 95 °C (5 atm pressure) in a PEMFC environment showed lowering of overpotential to the extent of 50 mV and concomitant enhancement of activity by greater than 2-fold [16]. Hydrodynamic voltammograms with rotating disks were used by Toda et al. [17–19] who reported enhancements to the extent of 10-fold using sputtered bimetallic films with Ni, Co and Fe. These have also been recently reported by Stamenkovic et al. [13] in their studies on thin layers of PtNi.

The enhancement of ORR electrocatalytic activity in the lower temperature PEM fuel system was first reported [16] on the basis of an investigation on a series of five binary alloys with Pt using the first row transition elements ranging from Cr to Ni. These results have been summarized in several reviews [20]. Further confirmation of enhancement in activity for ORR in PEM has been reported using supported Pt alloy electrocatalysts in a PEM fuel cell [21,22]. The role of alloying element in engendering enhancement of ORR catalytic activity in Pt based alloy catalysts has been ascribed to a decrease of the desorption free energy (ΔG_{ads}) of oxide species on Pt, particularly OH. The fact can be associated to the following effects: (i) electronic factors [23] (higher Pt 5d band vacancy for the alloys in the oxidized state); (ii) geometric effects [10] (shorter Pt–Pt bond distance and coordination number) and metal particle size effects [24]; (iii) other effects (ensemble effects [25], surface segregation effects [13], lower activity of water effect [26], etc.). These primarily effect OH_{ad} coverage [13] (θ_{ad} value effects, sacrificial elements oxidized leading to increase of available sites for O_{ads}). In brief these can be summarized as:

(a) The rate-determining step for oxygen reduction based on the wealth of prior data is considered to involve the initial adsorption by molecular oxygen (with or without a charge-transfer step) [20].

* Corresponding author.
E-mail address: s.mukerjee@neu.edu (S. Mukerjee).

0013-4686/$ – see front matter © 2009 Elsevier Ltd. All rights reserved.
doi:10.1016/j.electacta.2009.10.054

(b) The principal source of overpotential loss is due to deactivation of the surface as a result of oxide coverage on the Pt surface at and close to the open circuit potential due to water activation (oxidation) in the fully humidified environment of a PEM fuel cell. This is distinct from the PAFC's where the largely non-aqueous environment results in low water activity at the interface, however severe surface poisoning of the surface due to anion adsorption is responsible for poor kinetics [26–34].
(c) Alloying with transition metals such as Co, Cr, etc., have been shown to shift the onset of water activation and hence oxide coverage on the Pt surface. Several variants exist on the type of surface rendered after alloying, however general consensus is of a "skin" effect with the outer surface being predominantly Pt and an inner core comprising of the alloy [35].
(d) The primary change in electrocatalysis does not involve a lowering of the activation energy, but involves the pre-exponential term which is related to the coverage of oxides on the surface [27].

However, not sufficient work has been done on understanding the parallel pathways leading to peroxide yield. The peroxide intermediate H_2O_2 formed during oxygen reduction at the cathode of PEMFCs is believed to be the most important element for membrane degradation, reacting directly or with trace metal ions in the membrane/and carbon support to form hydroperoxy $HOO^{\bullet}$ and hydroxy $HO^{\bullet}$ radicals, which then attack the polymer [36,37]. The mechanism of hydroxyl radicals formation can be described using the following equations [38–40]:

$$O_2 + 2H^+ + 2e \rightarrow H_2O_2 \quad (1)$$

$$M^{2+} + H_2O_2 \rightarrow M^{3+} + {}^{\bullet}OH + OH^- \quad (2)$$

$$M^{3+} + H_2O_2 \rightarrow M^{2+} + {}^{\bullet}OOH + H^+ \quad (3)$$

Investigations towards H_2O_2 formation remain debatable due to a lot of undetermined variables [25,41–45]. Ziegelbauer et al. [46] prepared CoTMPP pyrolyzed at different temperatures and correlated chemical structures of the pyrolyzed reaction centers with peroxide yield. Combining rotating ring disk electrode (RRDE) measurements with an X-ray absorption $\Delta\mu$ technique, they found that the sample pyrolyzed at 800 °C containing a bulk $Co–N_2$ structure results in 10-fold increase in the peroxide yield in comparison with those pyrolyzed at lower temperature with $Co–N_4$ stoichiometry [46]. Murthi et al. [26] suggested that the Fe atoms on the surface of PtFe/C might cause to yield more H_2O_2. However, it was observed that Pt_3Co/C with more Co present on the surface gives lower peroxide current compared to Pt_2Co/C in Ramaswamy et al.'s degradation study of perfluorinated proton exchange membrane [47]. Furthermore, the production of H_2O_2 on the Pt_3Ni, Pt_3Co and "Pt-skin" alloy were found the same as on pure Pt by other researchers [13]. Therefore developing new synthesis method for PtM/C (M = Co, Ni, Fe, etc.) with capability to predict ORR kinetics and concomitant peroxide yield based on known crystal structure and surface composition is important form the perspective of attempts to designing cathodic catalysts and membrane interface for H_2/O_2 PEMFC.

In most of the methods [48–50] for preparation of carbon-supported Pt based alloy catalysts high temperature (over 900 °C) is required to form the alloy, resulting in a lower catalyst active area [48]. Another disadvantage of these traditional methods is that the Pt and other transition metals may deposit separately on carbon support, rather than in close association. Recently, a water-in-oil micro-emulsion media method has been reported as a good route to prepare nanoscaled catalysts [51,52]. Micro-emulsion method is widely used in production of metallic nanoparticles, semiconductor materials and nanometer-scale magnetic particles [53–57]. Micro-emulsion media (reverse micelle system) is made up of oil phase, surfactants and aqueous phase, in which polar groups of the surfactants are concentrated in the interior, and lipophilic groups extend outwards into the nonpolar solvent. Tiny well-defined droplets of water are encapsulated into reverse micelles. These reverse micelles are heterogeneous on a molecular scale; nevertheless they are thermodynamically stable. Reverse micelle system is a suitable reaction media for the synthesis of nanoparticles, because the inner aqueous phase inside these reverse micelles act as micro-reactors for performing simple synthesis reactions, maintaining size control (and thereby morphology) of micro-crystal products as determined by the size of these individual micelle [50,56]. The size of the micelle can be controlled by the molar water/surfactant ratio in the system [58]. Adjusting the water/surfactant ratio can form compartmentalized water droplets of different size, thus leading to careful control over the particle growth and the particle size. Carbon-supported platinum catalysts with a variety of particle sizes have been synthesized successfully by micro-emulsion method. Also, alloy of nanoparticles can be formed easily at room temperature in reverse micelle solutions [51,59]. These provide the twin advantage of size control and phase purity of the alloy formed.

In this paper, two reaction procedures, (a) simultaneous reduction and (b) sequential reduction associated with micro-emulsion method were used to synthesize PtCo/C catalysts. The former is aimed as a single step process leading to homogeneous alloy formation and the latter for core shell alloys with skin formation. These methods are aimed at providing insight on the mechanism of peroxide formation during ORR, i.e., the goal was to correlate alloy composition and surface structure to concomitant peroxide yield. This study was assisted by characterization using UV–vis, ICP-MS, XRD, TEM and SEM/DEX in conjunction with measurement of catalytic activity for oxygen reduction reaction (ORR). RRDE technique was used to simultaneously explore kinetics of ORR and peroxide formation on as-synthesized catalysts with various surface compositions. All investigations in this paper were aimed at comparing catalytic activity of PtCo/C catalysts synthesized in house with commercial Pt/C catalyst (BASF fuel cells, formerly E-TEK, Somerset, NJ, USA) for ORR in PEM fuel cells and relating peroxide yield to surface composition of PtCo alloy catalysts.

2. Experiment

2.1. Chemicals

Unless otherwise stated, all chemicals were of ACS reagent grade and used as received. The surfactant, sodium dioctyl sulfosuccinate (AOT), was obtained from Fisher scientific. Sodium borohydride ($NaBH_4$) was obtained from Sigma–Aldrich. Dihydrogen hexachloroplatinate(IV) hydrate ($H_2PtCl_6{\cdot}xH_2O$) was from Sigma–Aldrich. The cobalt source was cobaltous chloride ($CoCl_2$) from Alfa Aesar. The Ketjen carbon (BET surface area of 800 m^2/g) was dried at 100 °C in high vacuum oven before using. A commercially available catalyst of 30 wt% platinum supported on Vulcan XC72 was obtained from BASF fuel cells, formerly ETEK, Somerset, NJ, USA E-TEK.

2.2. Catalyst synthesis

Preparation of the Pt-Co nanoparticles was conducted using two micro-emulsion techniques as described in detail in a previous paper [59] i.e., by *simultaneous* and *sequential* methods. All reverse micelle solutions were prepared using cyclcohexane as the oil phase and AOT as the surfactant in the simultaneous procedure. The required amounts of 0.25 M H_2PtCl_6 and 0.25 M $CoCl_2$ were mixed and injected to a cyclohexane solution of AOT. The mixtures were then sonicated to form clear and stable micellar

solutions. The same procedure was used to prepare the reverse micelle solutions containing 1 M aqueous $NaBH_4$ solution as the reducing agent. Then the two reverse micelle solutions were mixed and vigorously stirred at room temperature for at least 4 h to ensure the complete reduction of H_2PtCl_6 as well as $CoCl_2$. The color of the solution changed to dark black from orange due to the formation of suspended metal nanoparticles.

Pt-Co nanoparticles were also prepared by a sequential reaction procedure. All solutions were made under the same conditions mentioned above. The solution (I) consisted of AOT, cyclohexane, and $CoCl_2$. The color of the solution is pink reflecting the color of Co^{2+} ion. The solution (II) contained AOT, cyclohexane and $NaBH_4$. The solution (III) had AOT, cyclohexane and H_2PtCl_6. The solution (I) and half of the solution (II) were mixed under constant stirring firstly, thereafter, the color of the solution changed to gray due to the suspended Co nanoparticles. Then the solution (III) and the rest of solution (II) were added to the above solution while being stirred for another 2 h.

An appropriate amount of Ketjen carbon was dispersed into cyclohexane and sonicated for over 1 h and then added to the as-prepared Pt-Co nanoparticles solutions. The slurry was vigorously stirred at room temperature for another 4 h. To break down the reverse micelles acetone was dropped slowly to the slurry inhibiting the agglomeration of platinum nanoparticles. The slurry was then filtered, washed with cyclohexane, acetone, ethanol, and water. The catalysts were dried in vacuum at 100 °C for 24 h. The carbon-supported PtCo/C prepared by simultaneous procedure and sequential procedure are hereafter designated as PtCo/C-S and PtCo/C-T. Temperature programmed heat treatment at 500 °C was carried out to all PtCo/C catalysts. These catalysts are denoted as Pt-Co/C-SH and Pt-Co/C-TH.

In order to investigate the effect of pH on the redox reactions in reverse micelles and crystal growth, the same procedures were performed in basic solution with adding stoichiometric amount of Na_2CO_3 to naturalize HCl produced. The catalysts are named as Pt-Co/C-SB and Pt-Co/C-TB, respectively. pH is expected to influence the structure, nucleation of the alloy process within the micelle.

2.3. Characterization

A Hewlett-Packard HP 8453 UV–vis spectrometer was used to record absorption spectra. The optical path length was 1.0 cm and 0.2 M AOT solutions were used as references.

Powder X-ray diffraction (XRD) patterns of the catalysts were taken on Rigaku X-ray Diffractometer equipment (D-Max-2000) with Cu Kα radiation. The particle size of the dispersed metal crystallites is estimated from the broadening of diffraction peaks using the Scherrer formula [60].

The morphology and particle size distribution of Pt were examined by a JEOL JEM-1000 general purpose transmission electron microscope (TEM). A small amount of PtCo/C-S or PtCo/C-T was dispersed in isopropanol and then applied on copper mesh with carbon film.

2.4. Electrode preparation and electrochemical measurements

Electrochemical measurements were conducted in a standard three-compartment electrochemical cell at room temperature using a rotating disk electrode (RDE) setup from Pine Instruments connected to an Autolab (Ecochemie Inc. Model-PGSTAT 30). A glassy carbon disk with geometric area of 0.19625 cm^2 was used as the substrate for deposition of catalyst films. All potentials were measured with respect to a sealed hydrogen reference electrode (RHE) made from the same electrolyte used in the ORR experiments. Before deposition of catalyst films, the RDE was first polished with 0.05 μm alumina slurry (Buehler, Lake Bluff, IL) and then cleaned with distilled water under sonication. All electrochemical experiments are carried out at room temperatures.

Table 1
Composition of PtCo/C catalysts prepared using micro-emulsion method.

Catalyst	Nominal composition		Composition from ICP analysis	
	Pt (wt%)	Pt:M (atomic)	Pt (wt%)	Pt:M (atomic)
Pt/C (E-TEK)	30	–	29.2	–
Pt-Co/C-S	26.4	67:33	22.4	79:21
Pt-Co/C-T	26.4	67:33	22.6	72:28
Pt-Co/C-SB	26.4	67:33	23.8	74:26
Pt-Co/C-TB	26.4	67:33	22.8	64:36

The composition of catalysts was analyzed by VG Elemental Plasmaquad-2 (PQ2) ICP-MS. The results can be seen in Table 1. It is apparent from the data (Table 1) that sequential micro-emulsion reduction technique is easier and more accurate in controlling the composition of the mixed metal nanoparticles. The higher discrepancy in atomic ratio of Pt and Co from the nominal value observed in the simultaneous method may be caused by the "competitive effect" during the reduction process. Co^{2+} ions are not supposed to have the equal chance to be reduced while in coexistence with $PtCl_6^{2-}$ ions in the reverse micelles solution.

The catalyst inks were prepared by dispersion of known amounts (according to the results of ICP) of catalyst powders (based on Pt content) into 20 ml of isopropanol and then sonicated for at least 30 min to reach a uniform suspension. The catalyst film was prepared by dispersing 8 μL of the catalyst ink on the glassy carbon (GC) substrate and dried at room temperature to reach a total Pt metal loading of 15 μg cm^{-2}. A diluted Nafion® solution (Water:Nafion is 50:1) was then applied on the catalyst film and dried in air. The Nafion® film was used as binder to prevent the loss of catalysts from the glassy carbon substrate during ORR measurements. There is evidence that the effect of very thin Nafion® film over the catalyst films is negligible to ORR measurements [61].

CVs were also taken in 1.0 mol L^{-1} KOH. Here a gold disk (9 mm in diameter) served as the substrate for working electrode and a platinum wire and Hg/HgO (KOH 1.0 mol L^{-1}) system were used as counter and reference electrode.

For RRDE measurement the preparation of inks and electrode preparation were similar to those of RDE measurement reported earlier [59]. The RRDE (Pine Instrument Company) consisted of a GC disk (5 mm in diameter) and a gold ring sealed in a polytetrafluoroethylene (PTFE) holder. The collection efficiency N determined using a solution of $[Fe(CN)_6]^{4-}/[Fe(CN)_6]^{3-}$ redox couple was 0.39. All RRDE experiments were performed in O_2 saturated 1 M $HClO_4$. The disk electrode potential was scanned between 1.2 V and 0.2 V vs. RHE at 20 mV/s, the ring electrode potential being held at 1.3 V vs. RHE where the H_2O_2 oxidation reaction was under diffusion control at all rotation rates [62]. The H_2O_2 portion was detected for different rotation rates (ω). The ring current at certain potential was proportional to $\omega^{1/2}$. Consequently, only one rotation rate is presented in this paper (ω = 900 rpm).

3. Results and discussion

3.1. UV–vis measurement

UV–vis measurement is a reliable way to confirm the formation of nanoparticles in micro-emulsions [6,63–65]. As can be seen in Fig. 1 two peaks (221 nm, 261 nm) are observed when both of $PtCl_6^{2-}$ and Co^{2+} are present within the confines of a micellar structure before reduction. These arise from the called "ligand-to-metal charge-transfer" absorption bands [66]. Corresponding spectra of these metals reduced separately using micellar methods described above are shown by their common peak at 210 nm. Simultaneous

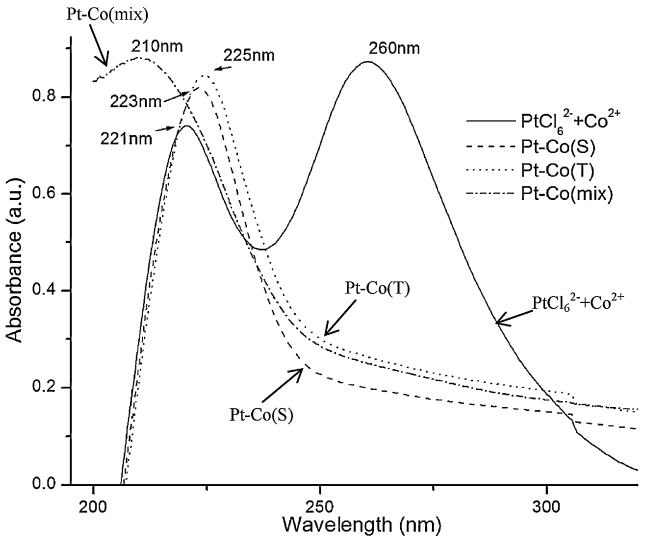

Fig. 1. UV–vis absorption spectra of micro-emulsion containing $PtCl_6^{2-}$, Co^{2+}; PtCo nanoparticles by both simultaneous procedure and sequential procedure; physical mixture of Pt and Co.

reductions of Pt and Co ions within the confine of micellar structure to yield the alloys using either *simultaneous* or *sequential* method yield corresponding peaks (223–225 nm) as shown in Fig. 1 confirming the presence of Pt-Co nanoalloys within the micelle. The peak positions of Pt-Co nanoalloy are significantly red shifted compared with physical mixture of micro-emulsions containing Pt and micro-emulsions containing Co (210 nm) due to the weaker plasma frequency in the ultraviolet range or interband transitions of Pt-Co nanoalloy [57,67].

3.2. TEM measurement

Representative TEM images of as-synthesized PtCo/C catalysts by micro-emulsion method are shown in Fig. 2(a and b) representing both sequential and simultaneous reductions. Histograms in Fig. 2(a and b) indicate a narrow particle size distribution for both Pt-Co/C-S and Pt-Co/C-T, thus enabling efficient control of particle size and morphology of the individual grains or crystallites. The average particle sizes of Pt-Co/C-S and Pt-Co/C-T are 3.4 nm and 2.9 nm, respectively. Both are evenly supported on the carbon, although there are some particles agglomerated on Ketjen Black EC-300J Carbon, see Fig. 2(a). Also, the differences in particle sizes and the microstructures of Pt-Co/C-S and Pt-Co/C-T are

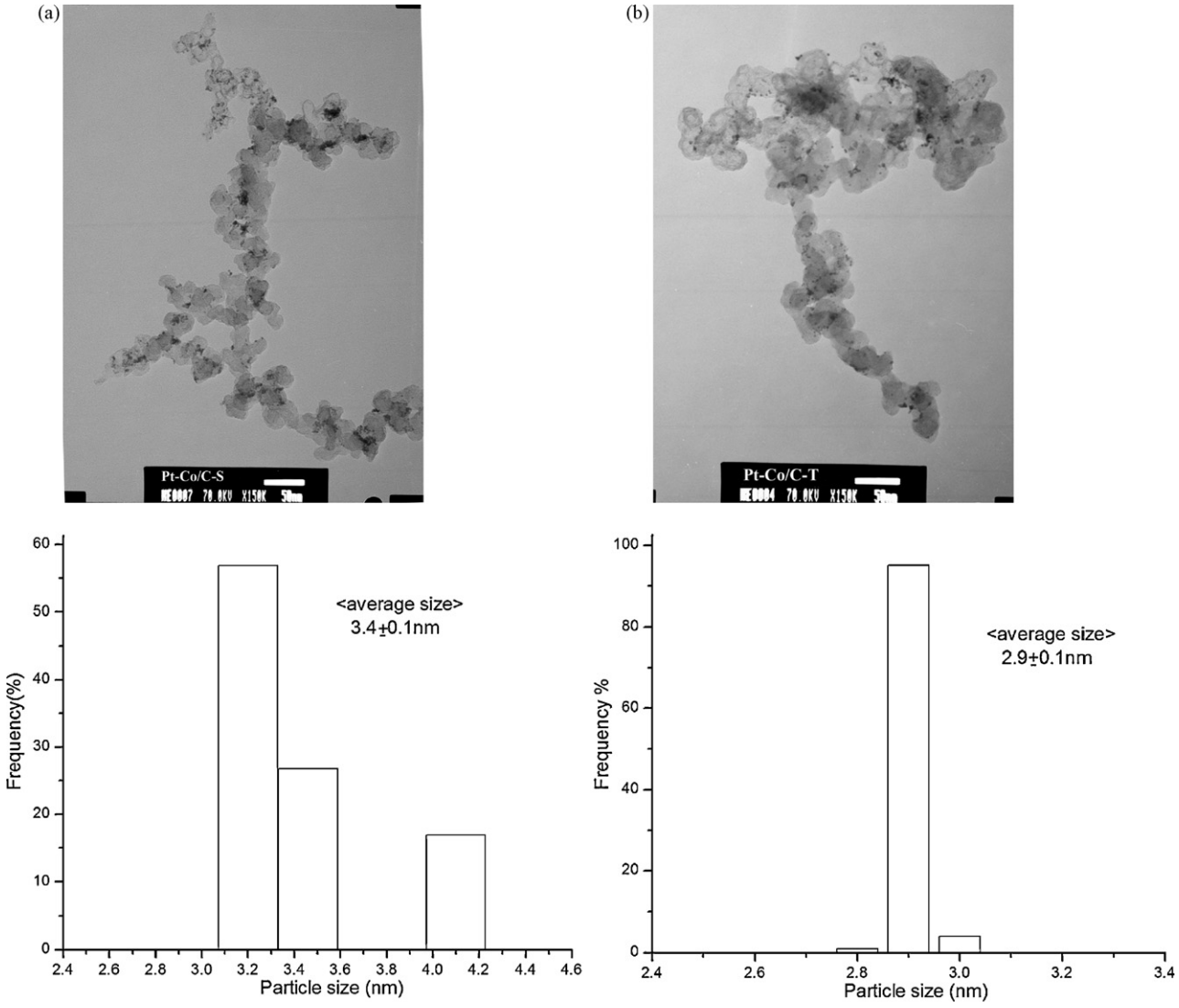

Fig. 2. (a) Transmission electron micrograph of PtCo/C-S and size distribution of platinum nanoparticles. (b) Transmission electron micrograph of PtCo/C-T and size distribution of platinum nanoparticles.

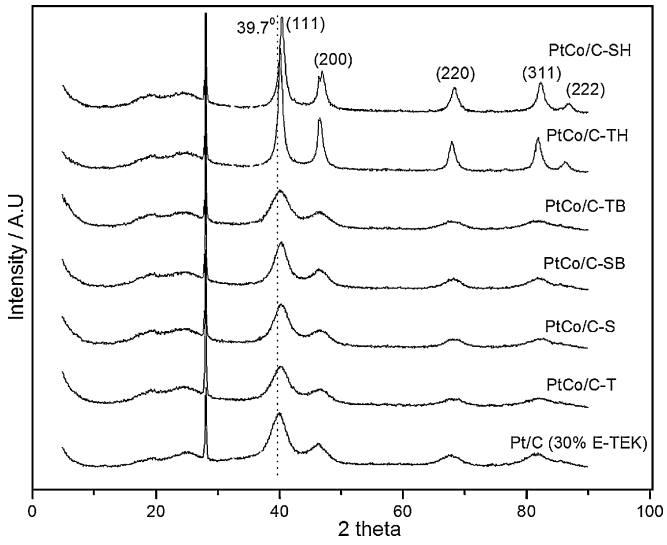

Fig. 3. X-ray diffraction patterns of Pt/C (30% E-TEK), PtCo/C-S, PtCo/C-T, PtCo/C-SB, PtCo/C-TB, PtCo/C-SH and PtCo/C-TH.

due to different nucleation and growth processes as a result of simultaneous and sequential methods. In the latter case, Co cores are formed first with smaller particle size in reverse micelles and separated. The smaller size of the Co cores can be discerned from the UV–vis peak at 210 nm in Fig. 1. Afterwards, Pt shells were produced surrounding these cores in a sequential manner. This lead to a smaller overall particle size (2.9 nm) as compared to those prepared in a simultaneous process (3.4 nm), as shown in Fig. 2.

3.3. XRD characterization

Fig. 3 shows the representative XRD patterns of the various catalysts synthesized. Both the positions and intensity were normalized by the peak at 28.037° caused by SiO_2 of glass holders. A broad peak at $2\theta \approx 25^\circ$ corresponds to diffraction due to carbon support [68]. The substitution of smaller Co atoms into Pt lattice causes shift of peaks to higher 2θ angles (see Table 2) as compared to Pt/C [16]. Lower shift could be seen for PtCo/C-T and PtCo/C-TB (sequential synthesis at higher pH environment) in Table 2, indicating that Co cores remain unalloyed and Co surface is enriched by Pt in the PtCo/C-T samples. This is also the same when the same sequential procedure is conducted at higher pH (no pH effect). Chen et al. [69] drew a similar conclusion during the study of nucleation and growth mechanism of Pd/Pt in micro-emulsion system, in which Pd cores were constituted followed by surface enrichment using Pt^{4+} salt in a micro-emulsion environment. In addition, there were no well-defined diffraction peaks suggesting the presence of any metallic Co or oxide phases. This is probably because the Co loading was very low and any metal Co species present were highly dispersed or amorphous [51].

XRD data was indexed and the diffraction patterns of all as-synthesized catalysts including those after heat treatment were found to be in accord with face centered cubic structure (*fm*3*m*). The samples after heat treatment exhibited higher intensity and sharper peaks indicative of larger crystallites and a comparably higher ordered structure.

The main diffraction peaks and lattice parameters for as-synthesized PtCo/C catalysts were summarized in Table 2. Regardless of difference of reaction conditions, lower extent of alloying could be seen for PtCo/C-T and PtCo/C-TB catalysts prepared by *sequential* method since lattice parameter and Pt–Pt bond distance show lower contraction compared to PtCo/C-S and PtCo/C-SB [16]. This is a good indication of the likelihood of successful formation of Co core with surface enriched Pt. However, the confirmation of this would depend on careful electrochemical measurements designed to determine extent of Co on catalysts prepared by sequential methods. These are enumerated in detail below (e.g. CVs in alkaline media, see Section 3.4).

The average crystallite size for PtCo/C catalysts and commercial catalyst was calculated using the Debye–Scherrer equation [60]:

$$Z = C\frac{\lambda}{B}\cos\theta \quad (4)$$

where Z is the diameter of the average particle size in Å; λ is the X-ray wavelength (1.5406 Å) for Cu Kα; θ is the Bragg angle; C is a factor (typically from 0.9 to 1.0) depending on crystallite shape; B is the full width at half maximum. It is interesting to note that smaller particles could be formed by sequential method as compared to those prepared using simultaneous method due to different nucleation and growth processes. The trends in particles size between XRD results and TEM measurements match very well.

3.4. Electrochemical characterization

Cyclic voltammograms (CVs) of all catalysts are shown in Fig. 4. They were obtained in 1 M $HClO_4$ between 0.035 and 1.1 V/RHE in order to avoid possible changes in Pt Electrochemical area (ECA) and surface composition [9]. The double layer of Pt/C (E-TEK) is the thinnest because Vulcan XC-72 carbon was used as support. The higher surface area of Ketjen carbon renders it more suitable to support metal prepared using micro-emulsion method. The high surface area and porous structure account for the slightly thicker double layer evident in the CVs. Furthermore, a redox couple can be seen at 0.6 V on the CV of PtCo/C-TH. This could be due to migration of reduced Co to the surface after heat treatment to PtCo/C-T in H_2/Ar mixture.

Additionally, it can be observed that H_{upd} region (weakly adsorbed) and peak potential of oxide reduction shift to positive potentials albeit to different extents for all catalysts prepared by micro-emulsion method in comparison with commercial Pt/C (E-TEK). Most important is the suppression of both features (H_{upd} and OH) in the case of PtCo-SH and SB samples prepared by simultaneous method. The suppression of oxide formation and positive shift in the corresponding reduction peak (see Fig. 4a) have been

Table 2
XRD data of PtCo/C catalysts by micro-emulsion method.

Catalyst	Lattice types	Pt (1 1 1) @2θ	Crystallite size/nm	Lattice parameter/Å	Pt–Pt bond distance/Å	Degree of alloying (%)[a]
Pt/C (E-TEK)	fcc	39.89	3.4	3.911	2.765	0
Pt-Co/C-S	fcc	40.33	3.9	3.870	2.737	71.9
Pt-Co/C-T	fcc	40.15	3.2	3.887	2.749	42.1
Pt-Co/C-SB	fcc	40.27	3.9	3.876	2.741	61.4
Pt-Co/C-TB	fcc	40.13	3.0	3.888	2.750	40.4
Pt-Co/C-SH	fcc	40.40	8.7	3.864	2.732	82.5
Pt-Co/C-TH	fcc	40.13	10.6	3.888	2.750	40.4

[a] degree of alloying was calculated from the expression: $\chi_a = (a - a_0)/(a_c - a_0)$[94].

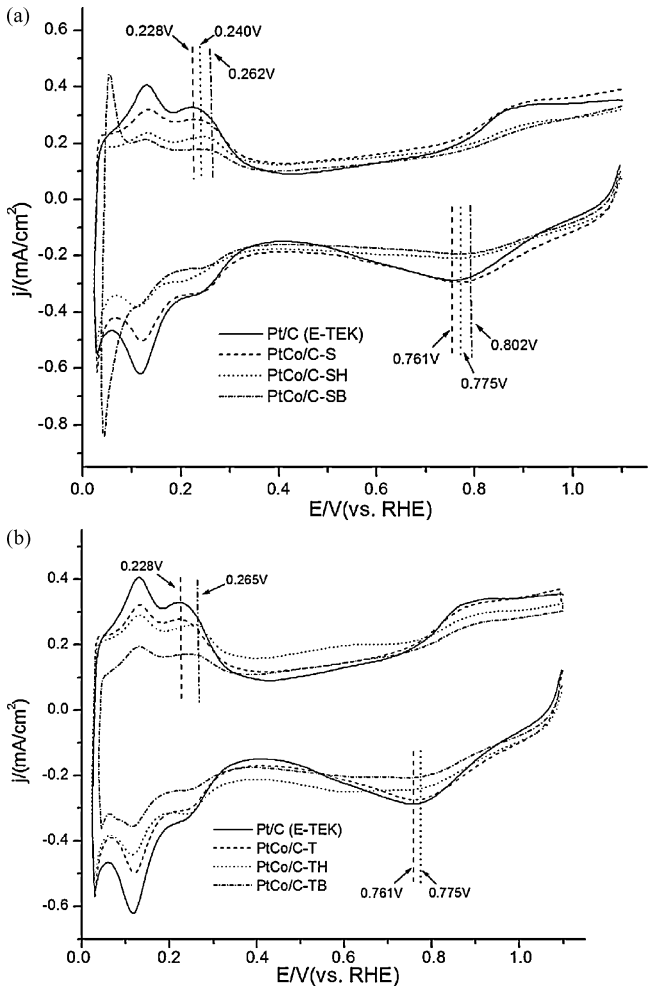

Fig. 4. (a) Cyclic voltammetry of Pt/C (E-TEK), PtCo/C-S, PtCo/C-SH and PtCo/C-SB at room temperature in Ar saturated 1 M $HClO_4$ at 50 mV/s, with 15 μg/cm² of Pt loading on the electrode. (b) Cyclic voltammetry of Pt/C (E-TEK), PtCo/C-T, PtCo/C-TH and PtCo/C-TB at room temperature in Ar saturated 1 M $HClO_4$ at 50 mV/s, with 15 μg/cm² of Pt loading on the electrode.

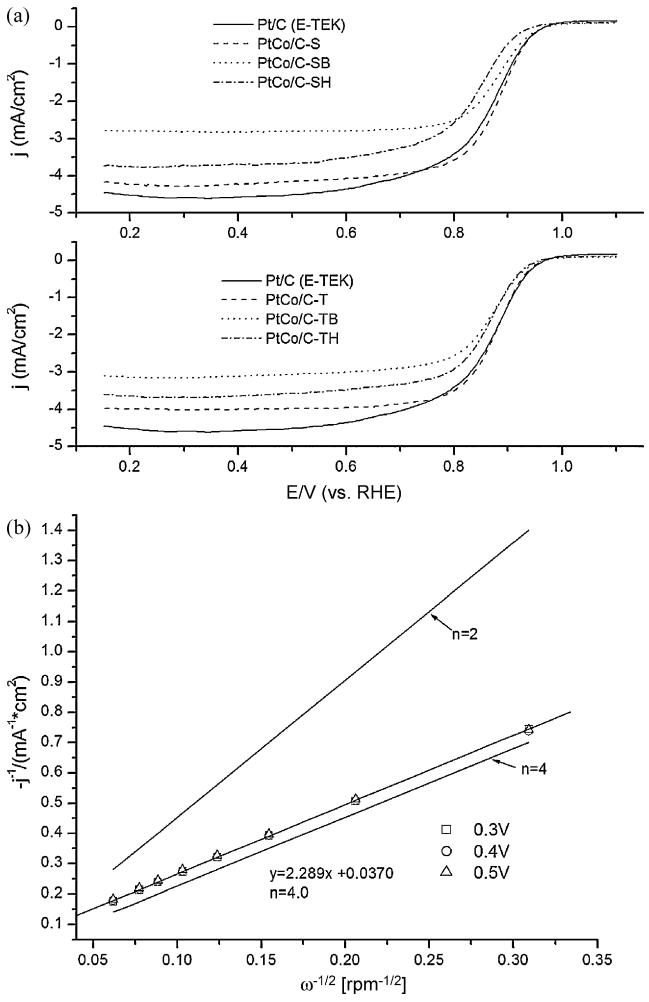

Fig. 5. (a) Disk currents density (based on geometric area of the electrode) obtained during the ORR on Pt/C (E-TEK), PtCo/C-S, PtCo/C-SH, PtCo/C-SB, PtCo/C-T, PtCo/C-TH and PtCo/C-TB at O_2 saturated 1 M $HClO_4$ at room temperature. Scan rate: 20 mV/s, with 15 μg/cm² of Pt loading on the electrode. (b) Koutecky–Levich plots at different potentials for ORR in the cathodic sweep on PtCo/C-S in O_2 saturated 1 M $HClO_4$ at room temperature. Scan rate: 20 mV s^{-1}.

previously reported and are indicative of lower activation of water and hence lower coverage of oxides on the Pt surface. The extent of presence of Co reported later in this paper however does affect this significantly. These have been reported earlier in more detail in refs. [26,70]. Inhibition of oxide formation on Pt in PtCo bimetallic crystallites either via a ligand effect (presence of subsurface Co with enriched Pt surface) or cooperative effect by surface Co in conjunction with Pt are both ascribed to be beneficial to oxygen [71].

Electrochemical surface area measurement (ECA) of Pt was calculated from both integration of the hydrogen adsorption and desorption peaks. Assuming a correlation value of 210 μC/cm² [72] average results of two independent measurements are tabulated in Table 3. Smaller ECA of PtCo/C-SH and PtCo/C-TH is in line with larger particle size after heat treatment. It is also interesting to note that PtCo/C-SB and PtCo/C-TB have smaller ECA than PtCo/C-S and PtCo/C-T even though the former exhibit similar particle size with the latter. The use of alkaline pH for preparation of these micelles appears to render the Pt surface to exhibit lower H_{upd} behavior. Fig. 5 shows disk polarization curves for the ORR on as-prepared catalysts at 1600 rpm, along with the kinetics analysis, presented in the form of the Kotecky–Levich plots. CV recorded in Ar purged solution was subtracted from ORR polarization current density at

Table 3
Electrode kinetic parameters for different catalysts in 1 M $HClO_4$ at room temperature. Scan rate: 20 mV s^{-1}, rotation rate: 1600 rpm.

Catalyst	ECA (m^2/g)	$E_{1/2}$ (V)	m	Mass activity (mA/μg Pt)			Specific activity (mA/cm²)			Tafel slope (mV/decade)
				@0.90 V	@0.85 V	@0.80 V	@0.90 V	@0.85 V	@0.80 V	
Pt/C (E-TEK)	36.2	0.864	1	0.115	0.401	0.900	0.315	1.105	2.475	151/60
Pt-Co/C-S	23.6	0.876	1	0.154	0.640	1.645	0.583	2.715	6.980	137/55
Pt-Co/C-T	24.0	0.871	1	0.109	0.479	1.242	0.452	1.995	5.175	123/56
Pt-Co/C-SB	11.6	0.880	1	0.151	0.742	2.725	1.445	6.400	23.55	95/64
Pt-Co/C-TB	9.2	0.870	1	0.102	0.464	1.285	1.105	5.035	13.95	118/64
Pt-Co/C-SH	14.6	0.842	1	0.054	0.287	1.030	0.370	1.640	4.975	119/62
Pt-Co/C-TH	15.5	0.863	1	0.093	0.422	1.315	0.600	2.715	8.490	115/62

Table 4
Number of exchanged electrons and H_2O_2 yield for different catalysts in 1.0 M $HClO_4$ at room temperature. Scan rate: 20 mV s^{-1}, rotation rate: 900 rpm.

Catalyst	Number of Exchanged electrons	*R* value	$\%H_2O_2$ [@0.6 V]	$\%H_2O_2$ [@0.7 V]
Pt/C (E-TEK)	3.7	N/A	1.18	0.699
Pt-Co/C-S	4.0	0.207	0.741	0.506
Pt-Co/C-T	3.8	0.167	0.618	0.448
Pt-Co/C-SB	3.5	0.251	1.42	0.972
Pt-Co/C-TB	3.7	0.207	1.23	0.797
Pt-Co/C-SH	3.9	0.211	0.878	0.451
Pt-Co/C-TH	3.8	0.231	0.954	0.480

the same sweep rate to eliminate the influence of the irreversible adsorption of oxides, perchlorate and charge of the electrical double layer on platinum [73]. In Fig. 5(a), three regions can be divided, namely, diffusion-controlled region (<0.65 V), mixed diffusion-kinetic limitation region (0.65–0.85 V) and Tafel region (>0.85 V). Similar results were obtained for all PtCo/C catalysts prepared by micro-emulsion method as well as commercial Pt/C catalyst. The ORR current *I* is expressed by Koutecky–Levich equation [61]:

$$\frac{1}{j} = \frac{1}{j_k} + \frac{1}{j_d} + \frac{1}{j_f} \quad (5)$$

$$j_d = 0.620nFD^{2/3}C_o\nu^{-1/6}\omega^{1/2} \quad (6)$$

where j_k is the kinetic current density, j_d is diffusion limiting current density, j_f is the diffusion-limited current density through the Nafion® film; *n* is the number of exchanged electron; ω is the angular frequency of rotation, $\omega = 2\pi f/60$, *f* is RDE rotation rate in rpm; *F* is the Faraday constant (96,485 C mol^{-1}), *D* is the diffusion coefficient of the molecular O_2 in 1 M $HClO_4$ solution (1.9×10^{-5} cm^2 s^{-1}), ν is the kinematic viscosity (9.87×10^{-3} cm^2 s^{-1}), C_O is the concentration of molecular oxygen (1.6×10^{-6} mol cm^{-3}).

The thickness of Nafion® film used to bind catalysts on the electrode is sufficiently small in that the resistance of it can be negligible [74]. As a result, Eq. (5) can be adjusted to simpler Eq. (7) without further need of the additional term:

$$\frac{1}{j} = \frac{1}{j_k} + \frac{1}{j_d} \quad (7)$$

Consequently, at select potentials, j^{-1} was plotted vs. $\omega^{-1/2}$ and straight lines could be obtained. The theoretical lines for 2-electron process of ORR and 4-electron process of ORR were also drawn in the same graph of Fig. 5(b). The number of exchanged electrons was calculated from the slope of straight lines. The n values of various catalysts in Table 4 were illustrative of the 4-electron charge-transfer pathway of ORR process on most of the electrocatalysts. Also, it implies the possibility that there is little isolated Co in as-synthesized catalysts since the transition metals are believed to cause part of H_2O_2, intermediate of oxygen reduction, not to be further reduced to H_2O, thereby introducing low *n* value [25,72].

Mass transport corrected Tafel plots (*E* vs. $\log|j_k|$) are shown in Fig. 6 for Pt/C (E-TEK) and PtCo/C prepared by the micro-emulsion method. In spite of the general transition in the Tafel slope, two Tafel regions were roughly defined around *RT/F* (~60 mV/decade) for the low overpotential range (*E* > 0.85 V) and 2*RT/F* (~120 mV/decade) for the high overpotential range (*E* < 0.80 V). The slopes of Tafel curve are usually indicative of pathways underlying ORR electrocatalysis [75]. In their series of kinetics studies of ORR on Pt and Pt based alloy catalysts, Markovic and co-workers [13,76] suggested that in $HClO_4$ where there is minimal specific anion adsorption, the Tafel slopes are controlled by both "energetic effects" (Temkin to Langmuir adsorption) [23,77] and "blocking effects" (surface coverage of OH controlling availability of O_2 adsorption) [78]. Tafel plots in Fig. 6 and slope values in Table 3 for PtCo/C-T, PtCo/C-TB as well as PtCo/C-TH prepared by the sequential method show quite similar ORR activity. This is interesting to note that from a mass activity perspective these electrocatalysts were either at par with Pt/C or were somewhat lower (Table 3). However, as the surface area of these electrocatalysts were on an average significantly lower as compared to Pt/C the specific activity normalized to electrochemically active Pt surface area was better. In contrast to the above similarity, larger differences of Tafel slopes could be seen for PtCo/C-S, PtCo/C-SH and PtCo/C-SB. In this case, there is considerable complexity in how cobalt was reduced competitively with Pt by $NaBH_4$ which may lead to such variation of the kinetics of ORR based on preparation conditions.

Mass activity and specific activity of as-synthesized catalysts and commercial catalyst towards ORR were summarized in Table 3 and also can be seen in Fig. 7. Some trends can be found: PtCo/C-SB > PtCo/C-S > PtCo/C-T ~ PtCo/C-TB ~ PtCo/C-TH > Pt/C (E-TEK) > PtCo/C-SH (mass activity); PtCo/C-SB > PtCo/C-TB > PtCo/C-TH ~ PtCo/C-S > PtCo/C-T ~ PtCo/C-SH > Pt/C (E-TEK) (specific activity). To different extents, catalytic performances of PtCo/C catalysts by the micro-emulsion method exhibit improvements over the commercial Pt/C catalyst. Again, reaction conditions in the process of synthesis need to be emphasized. Alkaline media seems to be more suitable for Pt and Co to coexist well albeit to some insoluble salt formation. In addition, heat treatment is commonly used to achieve good alloy of Pt and other transition metals [48–50,79]. However, heat treatment is not useful for PtCo/C-S by simultaneous reaction procedure to enhance its catalytic activity towards ORR, which suggests that Pt and Co are already in close intermetallic contact after reduction at room temperature. Notwithstanding, it is important to do the heat treatment for PtCo/C-T by the sequential reaction procedure because more than one phase might be formed after Pt was coated on Co surface (see results of XRD characterization in Section 3.3).

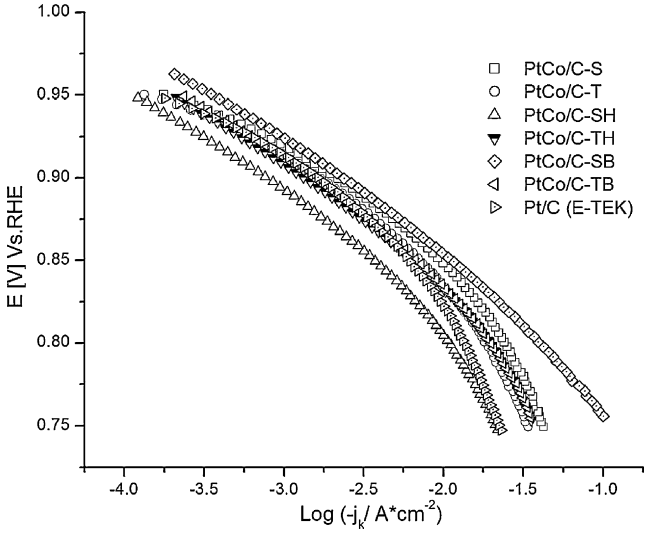

Fig. 6. Mass corrected Tafel plots of j_k for ORR obtained from disk current in the anodic sweep at 1600 rpm on PtCo/C catalysts by micro-emulsion method and Pt/C (E-TEK) catalysts. Scan rate: 20 mV s^{-1}.

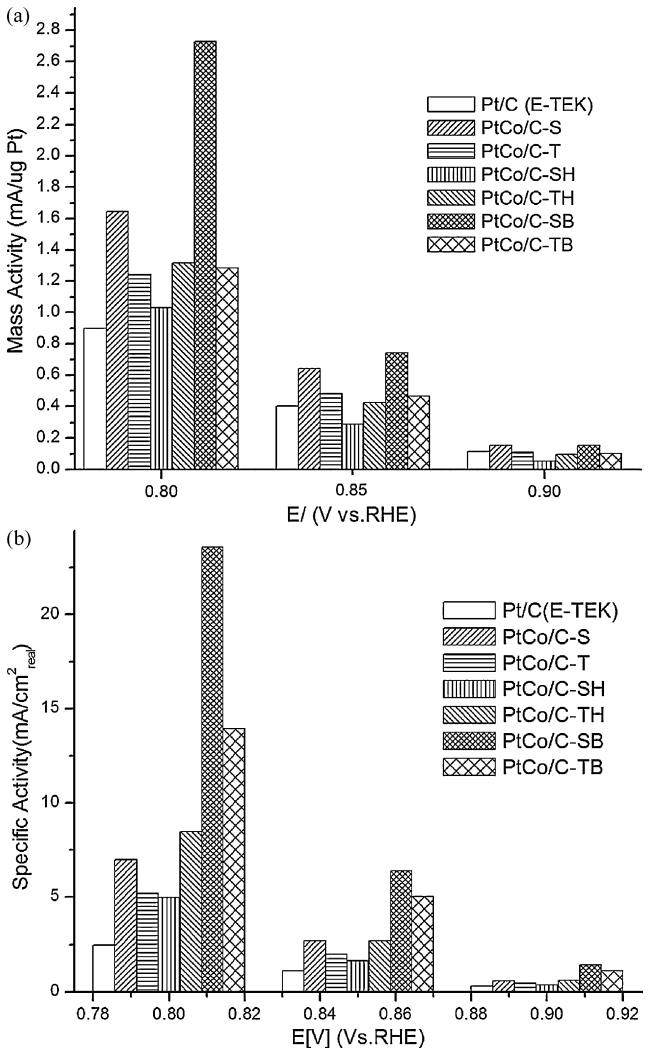

Fig. 7. (a) Mass activity of PtCo/C catalysts by micro-emulsion method and Pt/C (E-TEK) towards ORR at different potentials. (b) Specific activity of PtCo/C catalysts by micro-emulsion method and Pt/C (E-TEK) towards ORR at different potentials.

Redox-type processes involving the first row transition elements alloyed with Pt may be a reason for the enhanced ORR activity on PtM (M = transition metal) alloys catalysts as mentioned previously by us [80] and Stamenkovic et al.'s study of surface composition effects of PtM (M = Ni, Co) alloy on ORR [13]. Stamenkovic pointed out that transition metals may serve as "sacrificial" elements to be oxidized and inhibit the adsorption of OH_{ad} on Pt sites. Our results confirmed their plausible explanation as following. The reaction order (m) of ORR on as-synthesized catalysts was first checked from the slope of plots of $\log(i)$ vs. $\log(1 - i/i_d)$ [76]. From Fig. 8 and Table 3, the first order dependence of the kinetics of the ORR was performed on PtCo/C catalysts by the micro-emulsion method and commercial Pt/C. Therefore, the general rate expression can be seen in Eq. (8), assuming the first electron transfer for oxygen reduction ($O_{2(ad)} + e^- \rightarrow O^-_{2(ad)}$) is the rate-determining step:

$$i = nFKC_{O_2}(1 - m\theta_{ad})^x \exp\left(\frac{-\beta FE}{RT}\right) \exp\left(\frac{-\gamma r\theta_{ad}}{RT}\right) \quad (8)$$

where F is the Faraday's constant, K is the rate constant, C_{O2} is the concentration of O_2, m is the reaction order, θ_{ad} is the surface coverage of adsorbed intermediates, β and γ are symmetry factors, E is the applied potential, $r\theta_{ad}$ is a parameter related to the rate of

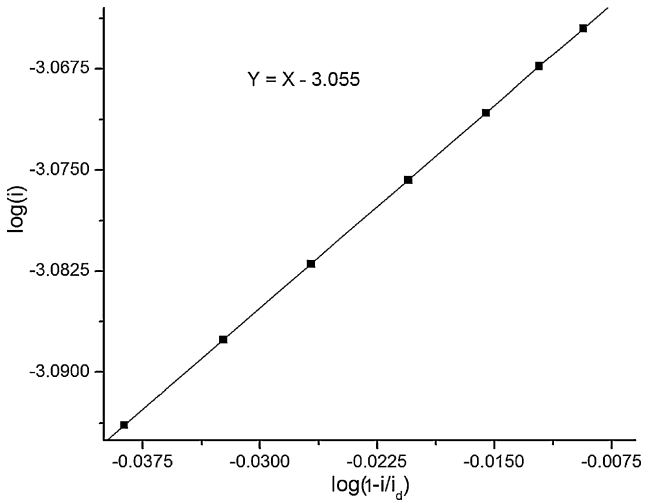

Fig. 8. Reaction order plot for oxygen reduction reaction on PtCo/C-SB in 1 M $HClO_4$. (The slope stands for the reaction order number.).

change of the apparent standard free energy of adsorption with the surface coverage of an oxide layer [13,26,81]. Since other parameters are identical to catalysts with different surface compositions, the item of $(1 - \theta_{ad})$ ($m = 1$) may control predominately the entire kinetics of ORR. The more available sites are for O_{ad}, the lower is the θ_{ad} value. Consequently, in $HClO_4$, the better inhibition of adsorption of OH on PtCo/C leads to higher possibility for O_2 to access to active sites on Pt surface and higher mass activity and eventually specific activity. From Table 3 the positive shift of both half-wave potential and peak potential of oxide reduction may be two criteria to confirm the redox-type process effect of cobalt as oxidizable "sacrificial" elements [13].

A representative set of ring currents obtained on a gold ring electrode during ORR on PtCo/C catalysts by prepared by micro-emulsion method and Pt/C (E-TEK) sample at 900 rpm are shown in Fig. 9. The relative amounts of H_2O_2 formed on the catalysts at typical operating potential in a fuel cell (0.6 V and 0.7 V) were shown in Table 4 based on the formula:

$$\chi_{H_2O_2} = \frac{2I_R/N}{I_D + I_R/N}, \quad N = 0.39 \quad (9)$$

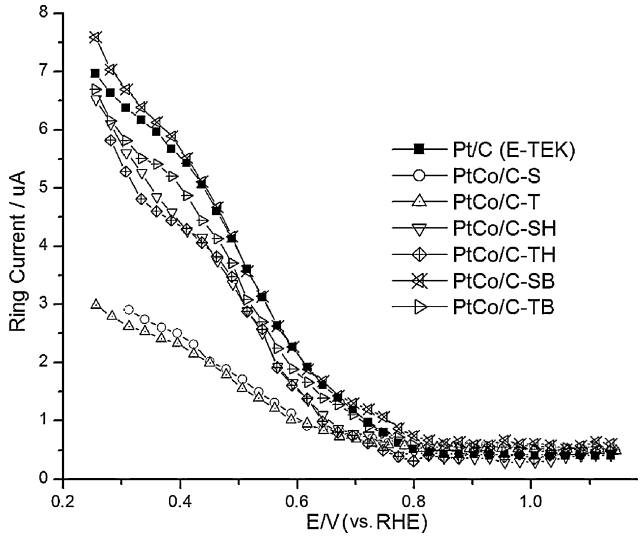

Fig. 9. Ring electrode current (I_R) (anodic sweep direction) during the ORR at 900 rpm on all PtCo/C catalysts by micro-emulsion method and commercial Pt/C in 1.0 M $HClO_4$ at a sweep rate of 20 mV/s.

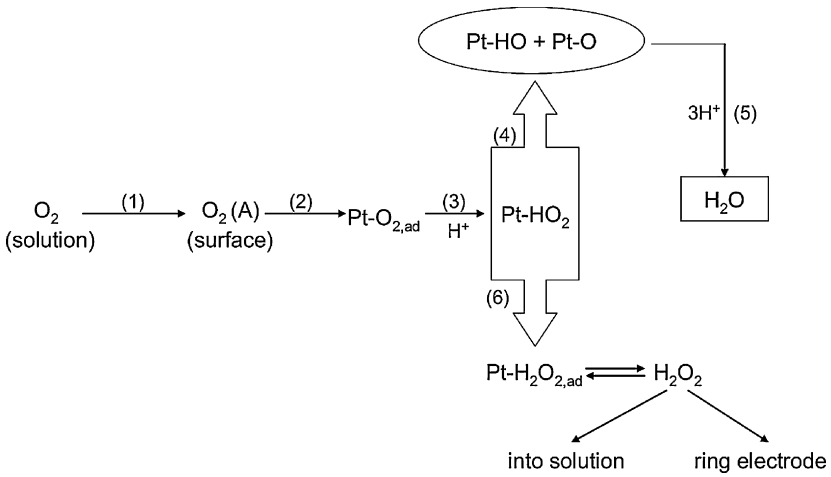

Fig. 10. Simplified sketch map of oxygen reduction reaction pathway.

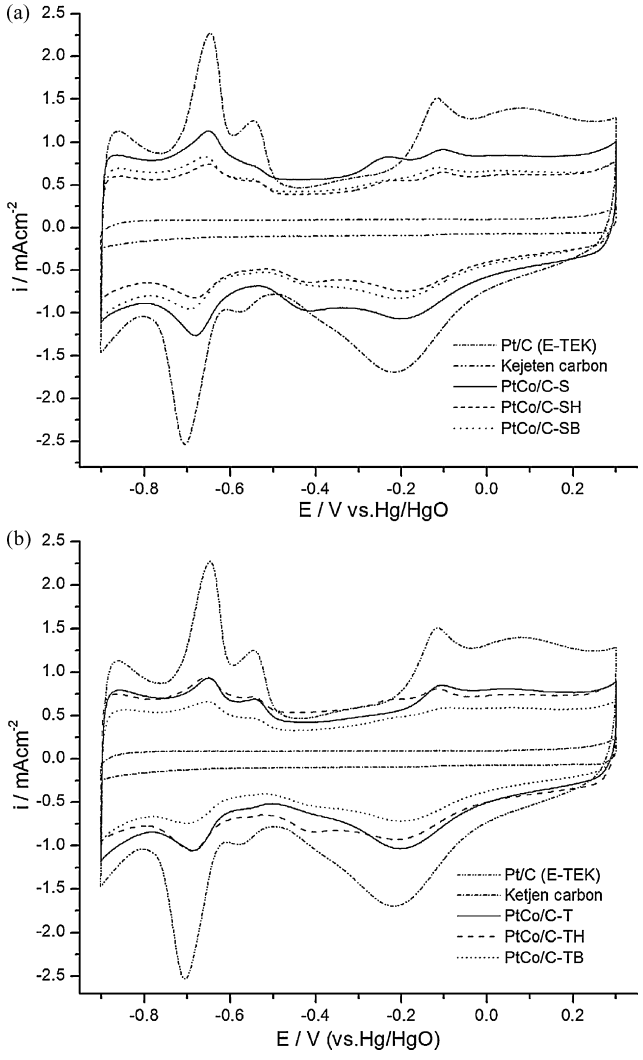

Fig. 11. (a) Cyclic voltammograms obtained for Pt/C (E-TEK), PtCo/C-S, PtCo/C-SH, PtCo/C-SB and ketjen carbon in 1.0 mol L^{-1} KOH at 50 mV s^{-1}. (b) Cyclic voltammograms obtained for Pt/C (E-TEK), PtCo/C-T, PtCo/C-TH, PtCo/C-TB, and Ketjen carbon in 1.0 mol L^{-1} KOH at 50 mV s^{-1}.

where N is the collection efficiency of the ring, χ is the mole fraction of peroxide formed, I_D and I_R are the disk and ring currents. From Fig. 9, the ring currents amount for a negligible percentage of the disk current above 0.6 V for all catalysts. It is not reasonable to correlate peroxide yield of ORR terms of individual parameters such as Pt particle size or changes in Pt–Pt bond distance, a more concerted effect involving a lot of variables as yet undetermined appears to be in effect. Antoine et al. [82] assumed that O_2 adsorption occurs via bridged end-on configuration on low coordination sites (atop edge and vertices) and leads to larger proportion of H_2O_2 production for catalysts with smaller particle size. The higher H_2O_2 yield was ascribed to this mode of adsorption as there was steric hindrance to dissociation of oxygen [82–84]. There may however remain competitive adsorption of bridge end-on O_2 and oxygenated species, in particular –OH, which poisons Pt as discussed earlier. In other words, the eventual number of bridge end-on O_2 moieties on smaller Pt particles may still be less than those on larger Pt particles since a large fraction of them are occupied by –OH and other oxygenated species. In the previous study from our group [47], smaller peroxide yield was found for ORR on Pt/C (30%) with smaller Pt particle size (2.7 nm in average) compared to Pt/C (60%) with larger Pt particle size (3.6 nm in average). Stamenkovic et al. [13] did not find any difference of production of H_2O_2 on the Pt_3Ni, Pt_3Co and "Pt-skin" in comparison with pure Pt. Various amounts of peroxide were also detected on different low index single crystal surface [85,86]. In addition, 4-fold enhancement of peroxide yield in 6 M TFMSA as compared to 1 M TFMSA was found in Murthi et al.'s study,[26] in which the high concentration (6 M) TFMSA provided the conditions of lower activity of water due to lower ratio of water and acid. As a result, comparisons were only made between samples prepared by simultaneous procedure as distinct from their counterparts prepared by sequential procedure, i.e. PtCo/C-S vs. PtCo/C-T; PtCo/C-SH vs. PtCo/C-TH; PtCo/C-SB vs. PtCo/C-TB. The results are tabulated in Table 4 and can be explained from the perspective of water activation and the formation of adsorbed oxygenated species (primarily Pt-OH). A possible description of reaction pathway of oxygen reduction reaction is proposed and can be seen in Fig. 10 [87,88]. Based on the conclusion by Sun and Tseung [89–92] that oxygen is mainly reduced via the series pathway with peroxide as the intermediate, catalysts with less "OH adsorption poisoning" are supposed to perform better towards ORR with more active sites available for H_2O_2 reversible adsorption and resulting in higher H_2O_2 yield which can be detected by RRDE technique. Their conclusion is in good agreement with our finding that the trend of MA of as-synthesized catalysts (PtCo/C-S > PtCo/C-T; PtCo/C-SB > PtCo/C-TB; PtCo/C-TH > PtCo/C-SH) is consistent

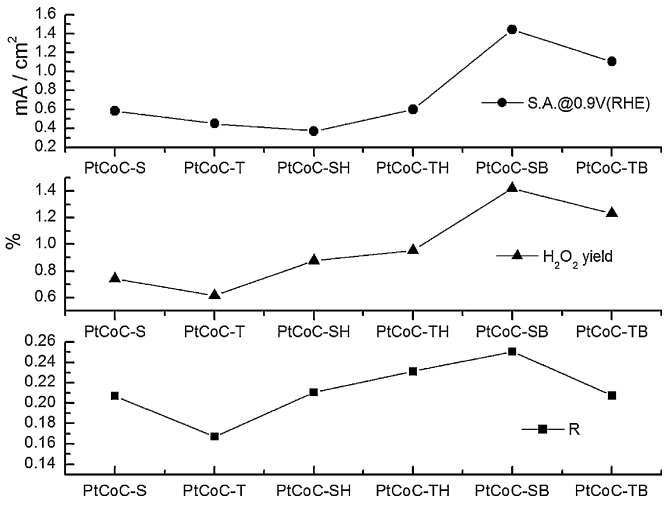

Fig. 12. *R* values (integrated charge of Co oxidized/integrated charge of H_{upd}), H_2O_2 yield at 0.6 V (vs. RHE) and specific activity (S.A.) at 0.9 V (vs. RHE) of PtCo/C by micro-emulsion method.

with the trend of peroxide yield (PtCo/C-S > PtCo/C-T; PtCo/C-SB > PtCo/C-TB; PtCo/C-TH > PtCo/C-SH).

Cyclic voltammograms in 1 M KOH as the methodology to probe surface composition for above catalysts are shown in Fig. 11. It is believed that a redox couple in the potential window of −0.2 V to −0.5 V vs. Hg/HgO is involved in the redox process relative to Co which is evident in the CV of PtCo/C-S [23]. Integration was made in the hydrogen UPD region (−0.78 V to −0.47 V vs. Hg/HgO) and oxide species of Co formation region (−0.37 V to −0.16 V vs. Hg/HgO). Ratios of charge of these two regions may reflect atomic ratio of Co and Pt (named R thereafter) on the surface of catalysts. These *R* values are more reflective of surface composition as opposed to those mentioned earlier which were bulk compositions (Table 1). The results can be found in Table 4 and Fig. 12. *R* values of PtCo/C-T and PtCo/C-TB are lower than those of their counterparts of PtCo/C-S and PtCo/C-SB due to different synthesis procedures (see Section 2.2). Higher *R* value of PtCo/C-TH than that of PtCo/C-SH suggested that migration of Co from inner layer to outer layer of both catalysts did happen during heat treatment process and the better contact of Pt and Co was gained for catalysts by simultaneous procedure. It is worthwhile to correlate *R* value with specific activity (SA) and peroxide yield for as-synthesized PtCo/C catalysts. It is evident that PtCo/C-S, PtCo/C-TH and PtCo/C-SB with higher *R* values have better catalytic activity towards ORR and consequently higher H_2O_2 yield than their counterparts' presumably due to sacrificial Co oxidized effect on inhibition of adsorption of OH as mentioned above. Further XPS, Auger electron spectroscopy (AES) experiments are needed to be done for the surface composition study in detail.

4. Conclusion

PtCo supported on carbon catalysts were synthesized in AOT/cyclohexane micro-emulsion in both acidic and basic media by reducing H_2PtCl_6 and $CoCl_2$ with $NaBH_4$. A modified sequential procedure was also used to synthesize PtCo/C and achieved lower Pt/Co ratio on the surface of the catalyst. UV–vis spectra of PtCo nanoparticles in reverse micelles showed difference from that of physical reverse micelle mixture of Pt and Co nanoparticles confirming intimate combination of Pt and Co as an intermetallic obtained at room temperature. PtCo particles of as-synthesized catalysts were nanoscale and uniformly distributed on the support. As determined from analysis of XRD patterns, PtCo/C-S and PtCo/C-SB prepared by simultaneous procedure have similar crystal structure and lattice parameters with PtCo/C-T and PtCo/C-TB prepared by sequential procedure. However, the latter showed smaller particle size and lower degree of alloying which lead to Co migration during high-temperature heat treatment. Better kinetics performance towards ORR was shown for PtCo/C synthesized by reverse micelle system comparing with the commercial Pt/C catalyst. PtCo/C-SB synthesized in alkaline media with simultaneous procedure shows the highest mass activity and specific activity. Insignificant peroxide yield was found for ORR on as-synthesized PtCo/C catalysts, which suggests that overwhelming ORR was undergoing a 4-electron pathway. *R* values representing a measure of Co surface composition were obtained from ratio of integration of oxidized peak related to Co and H_{upd} region of Pt. The results show good correlation with SA of different PtCo/C catalysts and H_2O_2 yield. The catalyst of PtCo/C-SB gives the highest peroxide yield along with the best performance towards ORR and highest presence of surface cobalt. A sacrificial Co oxidized effect on inhibition of adsorption of OH may be an explanation to higher catalytic properties and higher H_2O_2 yield of Pt based alloy catalysts.

Acknowledgements

The authors thank Bill Fowle and Nazih Hakim for the acquisition of the TEM images and the SEM images. The authors gratefully acknowledge the financial support of the Army Research Office under the auspices of a single investigator award.

References

[1] W. Vielstich, A. Lamm, H. Gasteiger, Handbook of Fuel Cells: Fundamentals, Technology, Applications, Wiley, 2003.
[2] V. Atrazhev, S.F. Burlatsky, N.E. Cipollini, D.A. Condit, N. Erikhman, ECS Trans. 1 (2006) 239.
[3] V.I. Birss, A.H.C. Sirk, S.A. Campbell, Proc. Electrochem. Soc. 31 (2002) 89.
[4] V. Mittal, H.R. Kunz, J.M. Fenton, ECS Trans. 1 (2006) 295.
[5] C. Perrot, L. Gonon, M. Bardet, C. Marestin, A. Pierre-Bayle, G. Gebel, Polymer 50 (2009) 1671.
[6] N. Li, B. Dong, W. Yuan, Y.A. Gao, L. Zheng, Y. Huang, S. Wang, J. Dispersion Sci. Technol. 28 (2007) 1030.
[7] E. Antolini, Mater. Chem. Phys. 78 (2003) 563.
[8] E. Antolini, R.R. Passos, E.A. Ticianelli, Electrochim. Acta 48 (2002) 263.
[9] H. Yang, W. Vogel, C. Lamy, N. Alonso-Vante, J. Phys. Chem. B 108 (2004) 11024.
[10] J.R.C. Salgado, E. Antolini, E.R. Gonzalez, J. Power Sources 141 (2005) 13.
[11] L. Xiong, A.M. Kannan, A. Manthiram, Electrochem. Commun. 4 (2002) 898.
[12] V. Raghuveer, P.J. Ferreira, A. Manthiram, Electrochem. Commun. 8 (2006) 807.
[13] V. Stamenkovicĭ, T.J. Schmidt, P.N. Ross, N.M. Markovic, J. Phys. Chem. B 106 (2002) 11970.
[14] S. Mukerjee, S. Srinivasan, J. Electroanal. Chem. 357 (1993) 201.
[15] S. Mukerjee, S. Srinivasan, M.P. Soriaga, J. McBreen, J. Phys. Chem. 99 (1995) 4577.
[16] S. Mukerjee, S. Srinvasan, M.P. Soriaga, J. Electrochem. Soc. 142 (1995) 1409.
[17] T. Toda, H. Igarashi, M. Watanabe, J. Electrochem. Soc. 145 (1998) 4185.
[18] T. Toda, H. Igarashi, H. Uchida, M. Watanabe, J. Electrochem. Soc. 146 (1999) 3750.
[19] T. Toda, H. Igarashi, M. Watanabe, J. Electroanal. Chem. 460 (1999) 258.
[20] R. Adzic, in: J. Lipkowski, P.N. Ross (Eds.), Recent Advances in the Kinetics of Oxygen Reduction, Electrocatalysis, Wiley-VCH, New York, 1998, p. 197.
[21] G. Tamizmani, G.A. Capuano, J. Electrochem. Soc. 141 (1994) 968.
[22] S. Gamburzev, O. Velev, S. Srinivasan, A.J. Appleby, F. Luczak, D. Wheeler, ECS Meeting Abstracts, Vol. MA 97-1, 1997, p. 626.
[23] F.H.B. Lima, M.J. Giz, E.A. Ticianelli, J. Braz. Chem. Soc. 16 (2005) 328.
[24] J.R.C. Salgado, E. Antolini, E.R. Gonzalez, J. Power Sources 138 (2004) 56.
[25] U.A. Paulus, A. Wokaun, G.G. Scherer, T.J. Schmidt, V. Stamenkovic, N.M. Markovic, P.N. Ross, Electrochim. Acta 47 (2002) 3787.
[26] V.S. Murthi, R.C. Urian, S. Mukerjee, J. Phys. Chem. B 108 (2004) 11011.
[27] B. Anderson Alfred, J. Roques, S. Mukerjee, S. Murthi Vivek, M. Markovic Nenad, V. Stamenkovic, J. Phys. Chem. B 109 (2005) 1198.
[28] J. Roques, A.B. Anderson, J. Electrochem. Soc. 151 (2004) E340.
[29] J. Roques, A.B. Anderson, J. Electrochem. Soc. 151 (2004) E85.
[30] J. Roques, A.B. Anderson, Proc. Electrochem. Soc. 30 (2003) 330.
[31] J. Roques, A.B. Anderson, Proc. Electrochem. Soc. 30 (2003) 10.
[32] J. Roques, A.B. Anderson, J. Fuel Cell Sci. Technol. 2 (2005) 86.
[33] J. Roques, A.B. Anderson, Surf. Sci. 581 (2005) 105.
[34] J. Roques, A.B. Anderson, V.S. Murthi, S. Mukerjee, J. Electrochem. Soc. 152 (2005) E193.
[35] M. Teliska, W.E. O'Grady, D.E. Ramaker, J. Phys. Chem. B 109 (2005) 8076.
[36] M. Inaba, 14th International Conference on the Properties of Water and Steam in Kyoto, 2004, p. 395.

[37] Q. Guo, P.N. Pintauro, H. Tang, S. O'Connor, J. Membr. Sci. 154 (1999) 175.
[38] E. Yeager, Electrochim. Acta 29 (1984) 1527.
[39] L. Zhang, C. Ma, S. Mukerjee, J. Electroanal. Chem. 568 (2004) 273.
[40] H. Liu, C. Song, L. Zhang, J. Zhang, H. Wang, D.P. Wilkinson, J. Power Sources 155 (2006) 95.
[41] M. Chatenet, M. Aurousseau, R. Durand, F. Andolfatto, J. Electrochem. Soc. 150 (2003) D47.
[42] U.A. Paulus, T.J. Schmidt, H.A. Gasteiger, R.J. Behm, J. Electroanal. Chem. 495 (2001) 134.
[43] N. Wakabayashi, M. Takeichi, H. Uchida, M. Watanabe, J. Phys. Chem. B 109 (2005) 5836.
[44] N. Wakabayashi, M. Takeichi, H. Uchida, M. Watanabe, Proc. Electrochem. Soc. 21 (2004) 124.
[45] H. Yano, J.M. Song, H. Uchida, M. Watanabe, J. Phys. Chem. C 112 (2008) 8372.
[46] J.M. Ziegelbauer, T.S. Olson, S. Pylypenko, F. Alamgir, C. Jaye, P. Atanassov, S. Mukerjee, J. Phys. Chem. C 112 (2008) 8839.
[47] N. Ramaswamy, N. Hakim, S. Mukerjee, Electrochim. Acta 53 (2008) 3279.
[48] G. Hoogers, Catalysts for the Proton Exchange Membrane Fuel Cell, CRC Press, 2003.
[49] M. Neergat, A.K. Shukla, K.S. Gandhi, J. Appl. Electrochem. 31 (2001) 373.
[50] D.H. Chen, J.J. Yeh, T.C. Huang, J. Colloid Interface Sci. 215 (1999) 159.
[51] L. Xiong, A. Manthiram, Electrochim. Acta 50 (2005) 2323.
[52] K. Wikander, H. Ekström, A.E.C. Palmqvist, A. Lundblad, K. Holmberg, G. Lindbergh, Fuel Cells 6 (2006) 21.
[53] A.E. Giannakas, A.K. Ladavos, P.J. Pomonis, Appl. Catal. B 49 (2004) 147.
[54] H. Boennemann, W. Brijoux, R. Brinkmann, R. Fretzen, T. Joussen, R. Koeppler, B. Korall, P. Neiteler, J. Mol. Catal. 86 (1994) 129.
[55] M.-L. Wu, D.-H. Chen, T.-C. Huang, Langmuir 17 (2001) 3877.
[56] H.H. Ingelsten, R. Bagwe, A. Palmqvist, M. Skoglundh, C. Svanberg, K. Holmberg, D.O. Shah, J. Colloid Interface Sci. 241 (2001) 104.
[57] M. Pileni, Adv. Colloid Interface Sci. 46 (1993) 139.
[58] K. Holmberg, B. Jönsson, B. Kronberg, B. Lindman, Surfactants and Polymers in Aqueous Solution, 2nd ed., John Wiley & Sons, Chichester, 2002.
[59] Y. Qian, W. Wen, P.A. Adcock, Z. Jiang, N. Hakim, M.S. Saha, S. Mukerjee, J. Phys. Chem. C 112 (2008) 1146.
[60] B.D. Cullity, S.R. Stock, Elements of X-ray Diffraction, 3rd ed., Prentice Hall, Upper Saddle River, NJ, 2001.
[61] E. Higuchi, H. Uchida, M. Watanabe, J. Electroanal. Chem. 583 (2005) 69.
[62] S.L. Gojkovic, S. Gupta, R.F. Savinell, Electrochim. Acta 45 (1999) 889.
[63] M. Ethayaraja, C. Ravikumar, D. Muthukumaran, K. Dutta, R. Bandyopadhyaya, J. Phys. Chem. C 111 (2007) 3246.
[64] W. Zhang, X. Qiao, J. Chen, Mater. Chem. Phys. 109 (2008) 411.
[65] W.-z. Zhang, X.-l. Qiao, L.-l. Luo, J.-g. Chen, Guangpuxue Yu Guangpu Fenxi 29 (2009) 789.
[66] B. Shelimov, J.-F. Lambert, M. Che, B. Didillon, J. Catal. 185 (1999) 462.
[67] P.D.I. Fletcher, A.M. Howe, B.H. Robinson, J. Chem. Soc. Faraday Trans. I 83 (1987) 985.
[68] A.S. Aricò, V. Antonucci, N. Giordano, A.K. Shukla, M.K. Ravikumar, A. Roy, S.R. Barman, D.D. Sarma, J. Power Sources 50 (1994) 295.
[69] C.H. Chen, B.J. Hwang, G.R. Wang, L.S. Sarma, M.T. Tang, D.G. Liu, J.F. Lee, J. Phys. Chem. B 109 (2005) 21566.
[70] M. Teliska, V.S. Murthi, S. Mukerjee, D.E. Ramaker, J. Electrochem. Soc. 152 (2005) A2159.
[71] K.J.J. Mayrhofer, B.B. Blizanac, M. Arenz, V.R. Stamenkovic, P.N. Ross, N.M. Markovic, J. Phys. Chem. B 109 (2005) 14433.
[72] E.M. Crabb, R. Marshall, D. Thompsett, J. Electrochem. Soc. 147 (2000) 4440.
[73] Y. Takasu, N. Ohashi, X.-G. Zhang, Y. Murakami, H. Minagawa, S. Sato, K. Yahikozawa, Electrochim. Acta 41 (1996) 2595.
[74] H.R. Colón-Mercado, B.N. Popov, J. Power Sources 155 (2006) 253.
[75] H. Xu, Y. Song, H.R. Kunz, J.M. Fentona, J. Electrochem. Soc. 152 (2005) A1828.
[76] N.M. Markovic, R.R. Adzic, B.D. Cahan, E.B. Yeager, J. Electroanal. Chem. 377 (1994) 249.
[77] M.T. Giacomini, E.A. Ticianelli, J. McBreen, M. Balasubramanianb, J. Electrochem. Soc. 148 (2001) A323.
[78] N.M. Markovic, T.J. Schmidt, V. Stamenkovic, P.N. Ross, Fuel Cells 1 (2001) 105.
[79] V.M. Jalan, in: U.S. Patant (Ed.), Noble Metal/Vanadium Alloy Catalyst and Method for Making, United Technologies Corporation, 1980.
[80] M. Teliska, D.E. Ramaker, V. Srinivasamurthi, S. Mukerjee, Proc. Electrochem. Soc. 30 (2003) 212.
[81] U.A. Paulus, A. Wokaun, G.G. Scherer, T.J. Schmidt, V. Stamenkovic, V. Radmilovic, N.M. Markovic, P.N. Ross, J. Phys. Chem. B 106 (2002) 4181.
[82] O. Antoine, R. Durand, J. Appl. Electrochem. 30 (2000) 839.
[83] G. Kokkinidis, D. Jannakoudakis, J. Electroanal. Chem. 162 (1984) 163.
[84] J.C. Huang, R.K. Sen, E. Yeager, J. Electrochem. Soc. 126 (1979) 786.
[85] C.F. Zinola, A.M. Castro Luna, W.E. Triaca, A.J. Arvia, J. Appl. Electrochem. 24 (1994) 119.
[86] C.F. Zinola, W.E. Triaca, A.J. Arvia, J. Appl. Electrochem. 25 (1995) 740.
[87] S. Chen, A. Kucernak, J. Phys. Chem. B 108 (2004) 3262.
[88] Q. Zha, Introduction of Electrode Kinetics, 3rd ed., Science Press, Beijing, 2002.
[89] Z. Sun, A.C.C. Tseung, Electrochem. Solid-State Lett. 3 (2000) 413.
[90] Z. Sun, A.C.C. Tseung, Electrochem. Solid-State Lett. 4 (2001), L2-L2.
[91] Z. Sun, H.C. Chiu, A.C.C. Tseung, Electrochem. Solid-State Lett. 4 (2001) E9.
[92] H.C. Chiu, A.C.C. Tseung, Electrochem. Solid-State Lett. 2 (1999) 379.